Quantitative interaction analysis permits molecular insights into functional NOX4 NADPH oxidase heterodimer assembly

Received for publication, November 20, 2017, and in revised form, April 4, 2018 Published, Papers in Press, April 19, 2018, DOI 10.1074/jbc.RA117.001045

Sharon O'Neill[‡§1], Magalie Mathis[¶], Lidija Kovačič[‡§2], Suisheng Zhang[‡§], Jürgen Reinhardt[¶], Dimitri Scholz[‡], Ulrich Schopfer[¶], Rochdi Bouhelal[¶], and Ulla G. Knaus[‡§3]

From the [‡]Conway Institute and [§]School of Medicine, University College Dublin, Dublin 4, Ireland and the [¶]Novartis Institutes for Biomedical Research, 4002 Basel, Switzerland

Edited by Karen G. Fleming

Protein–protein interactions critically regulate many biological systems, but quantifying functional assembly of multipass membrane complexes in their native context is still challenging. Here, we combined modeling-assisted protein modification and information from human disease variants with a minimal-size fusion tag, split-luciferase–based approach to probe assembly of the NADPH oxidase 4 (NOX4)-p22^{phox} enzyme, an integral membrane complex with unresolved structure, which is required for electron transfer and generation of reactive oxygen species (ROS). Integrated analyses of heterodimerization, trafficking, and catalytic activity identified determinants for the NOX4-p22^{phox} interaction, such as heme incorporation into NOX4 and hot spot residues in transmembrane domains 1 and 4 in p22^{phox}. Moreover, their effect on NOX4 maturation and ROS generation was analyzed. We propose that this reversible and quantitative protein–protein interaction technique with its small split-fragment approach will provide a protein engineering and discovery tool not only for NOX research, but also for other intricate membrane protein complexes, and may thereby facilitate new drug discovery strategies for managing NOX-associated diseases.

Protein–protein interactions (PPIs)[4] are vital for the regulation of biological systems. Current methods in unperturbed cellular environments rely mostly on antibodies, fluorescent tags, or fragment complementation. Pitfalls are often antibody specificity and sensitivity, tag-induced changes in protein localization and function, or the absence of dynamic quantification. Understanding and interfering with dimer formation of multipass receptors, transporters, or enzyme complexes containing numerous interhelical contacts may be feasible by reversible split-luciferase complementation assays (1), but it is often impeded by the sensitivity of the functional conformation to tag-induced perturbations. Newly developed approaches such as reversible protein-fragment complementation coupled with stability-optimized bright luminescence may permit detailed analysis of assembly and disassembly of these complexes in living cells (2).

Assembly of multipass integral membrane enzymes or receptors by homo- or heterodimerization is governed by the folding and packing of their transmembrane segments, thereby enabling PPIs within the membrane, which directly participate in stabilization of the complex and signal transduction across lipid bilayers. Reactive oxygen species producing NADPH oxidases form membrane-bound complexes composed of 1–5 minimally required components. The ability to transfer electrons from NADPH across the membrane to molecular oxygen resides in several distinct features of the catalytic NOX domain but requires also in all NADPH oxidases (except for NOX5; NOX1–4 and DUOX1–2) heterodimerization with specific integral membrane proteins (p22^{phox}, DUOXA1–2). Heterodimerization is required for NOX/DUOX stabilization and exit from the endoplasmic reticulum and may direct intracellular trafficking (3). *In vivo* mechanistic analysis of heterodimerization is particularly difficult for NADPH oxidases, as the complex structure is unresolved, and enzyme activity is easily impaired by amino acid changes, insertions, or additions. If interference with the ability to heterodimerize or to disrupt the formed complex could be achieved, it might lead to a new class of NOX inhibitors.

The NADPH oxidase NOX4, a primarily transcriptionally regulated, constitutively active enzyme that generates H_2O_2 (4), is a promising drug target for fibrotic and metabolic disease (5). Heterodimer formation of NOX4 (6 transmembrane α-helices (TMHs)) with p22^{phox} (4 TMHs) in the endoplasmic reticulum is thought to occur after incorporation of two bis-histidine–coordinated low-potential hemes, followed by dimer trafficking to the plasma membrane or, in some cell types, to intracellular membrane compartments. To date, NOX mutagenesis/chimera studies or rare human loss-of-function variants (*CYBA* (p22^{phox}), *CYBB* (NOX2), and *NOX1*) provide the only information about particular residues or structural elements of the NOX1–4 heterodimers required for NOX activity. NOX4-dependent H_2O_2 generation is contingent on heterodimerization, NADPH/FAD binding, electron transfer across the membrane via heme to molecular oxygen, and intramolecular conversion

This work was supported by a grant from the Science Foundation Ireland (to U. G. K.). The authors declare that they have no conflicts of interest with the contents of this article.

This article contains Figs. S1–S3.

[1] Part of the MolCellBiol Programme (Programme for Research in 3rd-Level Institutions, co-funded under the EU Regional Development Fund).

[2] Present address: Novartis Pharmaceuticals, Elm Park Business Campus, Merrion Rd., Dublin 4, Ireland.

[3] To whom correspondence should be addressed: Conway Institute, University College Dublin, Belfield, Dublin 4, Ireland. Tel.: 353-1-7166719; E-mail: ulla.knaus@ucd.ie.

[4] The abbreviations used are: PPI, protein-protein interaction; TMH, transmembrane α-helix; DPI, diphenyleneiodonium; NOX, NADPH oxidase; PDB, Protein Data Bank; aa, amino acid(s); HVA, homovanillic acid; RLU, relative light unit(s); ANOVA, analysis of variance.

of superoxide to H_2O_2 by an unidentified structure-induced mechanism. Reactive oxygen species generation and NADPH/oxygen consumption are the only quantifiable readouts for the catalytic activity of all NOX/DUOX enzymes, impeding molecular insight into unique contacts at PPI interfaces that could be exploited for selective NOX isoform targeting. Here, we describe dynamic quantification of NOX4-p22^{phox} assembly in a cellular and functional context, leading to discovery of hot spot residues and interaction surfaces required for heterodimerization.

Results

Development of a NOX4-p22^{phox} PPI assay

Understanding NOX4 heterodimerization is hindered by lack of structural information. We and others have attached tags at the enzyme's N or C termini. NOX4 activity tolerates some short (V5) (6) or large (GFP) (7) N-terminal tags, albeit only certain sequences permit maturation and can be visualized. The partner protein p22^{phox} can be modified at the C terminus without loss of expression or its ability to heterodimerize with NOX2 (8). Ambasta *et al.* (9) used C-terminal NOX4-yellow fluorescent protein and p22^{phox}-cyan fluorescent protein fusions for FRET studies. We and others postulated that the first intracellular loop (B-loop) and the penultimate C-terminal region of NOX4 form an interface required for enzymatic activity (10–12), a scenario that would exclude NOX4 C-terminal additions. Indeed, a C-terminal GFP fusion markedly reduced NOX4 expression and H_2O_2 generation (Fig. 1) independently of linker length or linker composition (not shown). Thus, quantitative and functional PPI analysis of NOX4-p22^{phox} and other NOX isoform complexes will require reducing the size of fusion tags as recently accomplished by the reversible split-luciferase complementation assay NanoBiT® (SB-11aa, LB-157aa) (2) and strategically placing these fusions without disrupting any of the structural features required for NOX4 function.

By combining structure–function information and homology modeling of the NOX4-p22^{phox} complex, SB/LB additions or sequence replacements were designed for NOX4 and p22^{phox}, including variation of length and composition of linkers. A total of 31 SB/LB-containing NOX4 or p22^{phox} constructs were co-transfected with their WT dimerization partner for expression and functional analysis (Fig. S1, *A–F*; not all fusions shown). The most promising pairs were combined (SB/LB) and retested for catalytic activity (Fig. S1, *G* and *H*). We then chose two H_2O_2-generating (SB1-NOX4/p22-LB2 and NOX4-SB5/p22-LB2) and a negative pair (NOX4-SB6/p22-LB2) for NanoLuc PPI detection (Fig. 2*A*). SB1-NOX4/p22-LB2 elicited a strong signal, whereas NOX4-SB5/p22-LB2 and NOX4-SB6/p22-LB2 did not generate luminescence (Fig. 2*B*). Shortening the linker between SB and NOX4 (SB2-NOX4/p22-LB2) moderately reduced luminescence, whereas deletion of the last 23 amino acid residues of p22^{phox}, increasing p22-LB2 linker length, or changing linker composition was inconsequential (Fig. S2). Co-expression of functional SB/LB pairs increased their protein expression, catalytic activity, and cell-surface expression (Fig. 2, *C–E*), probably due to heterodimer stabilization. In conclusion, we identified several optimal SB/LB combinations (SB1/SB2-NOX4/p22-LB1, -LB2, and -172LB) that formed a functional NOX4 enzyme complex at the cell surface.

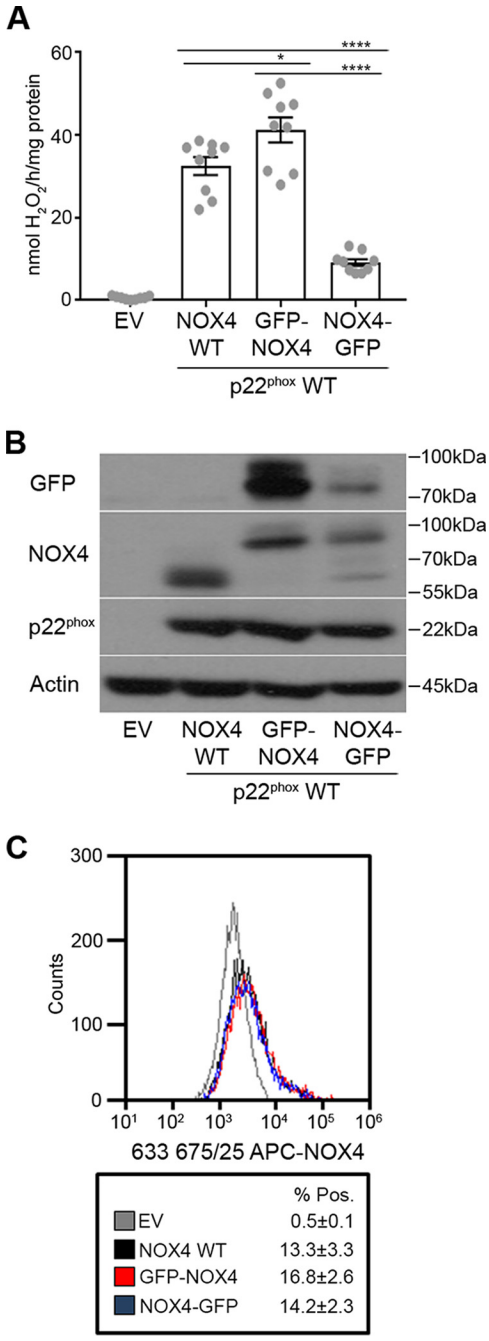

Figure 1. C-terminal GFP fusion decreases NOX4 enzymatic activity. *A*, catalytic activity (H_2O_2 release) of N- and C-terminal NOX4 fusion proteins. *Error bars*, S.E; one-way ANOVA with post hoc Tukey's multiple-comparison test. *B*, expression analysis of proteins (immunoblotting GFP, NOX4, p22^{phox}, and actin). *C*, cell-surface localization (flow cytometry with anti-NOX4 antibody). ****, $p \leq 0.001$.

SB incorporation into the second cytosolic loop (D-loop) of NOX4 (SB3 and SB4) was not tolerated (Fig. S1*B*), supporting D-loop involvement in heterodimerization (6). Replacement of penultimate C-terminal NOX4 sequences with SB abolished H_2O_2 production (Fig. S1*B*), whereas insertion of SB between FAD_2 and $NADPH_1$ (SB5) permitted enzyme trafficking and catalytic activity. This indicates that the SB5-containing com-

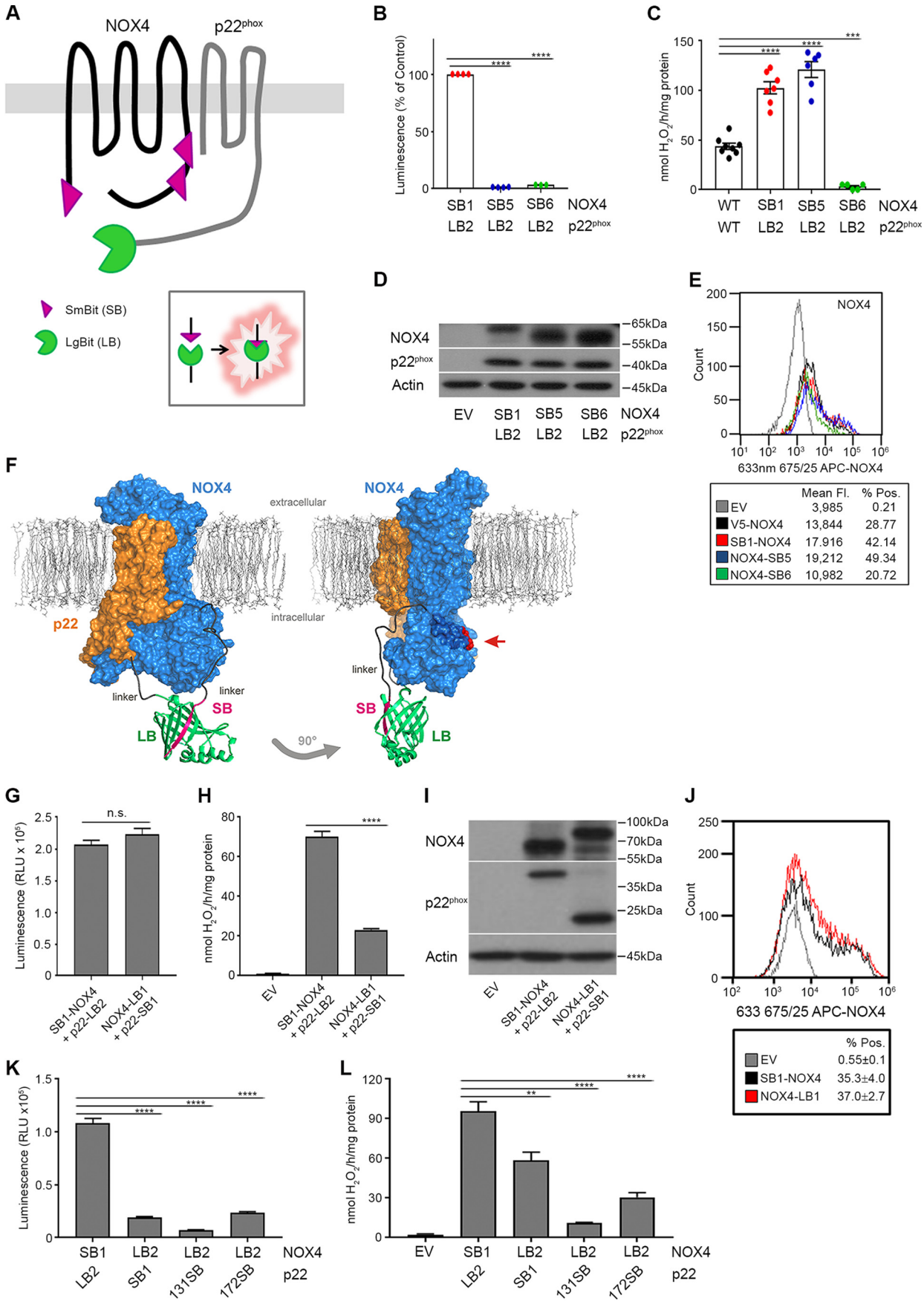
A
NOX4
p22phox
SmBit (SB)
LgBit (LB)
B
Luminescence (% of Control)
SB1 LB2
SB5 LB2
SB6 LB2
NOX4 p22phox
C
nmol H2O2/h/mg protein
WT WT
SB1 LB2
SB5 LB2
SB6 LB2
NOX4 p22phox
D
NOX4
p22phox
Actin
65kDa
55kDa
40kDa
45kDa
EV
SB1 LB2
SB5 LB2
SB6 LB2
NOX4 p22phox
E
NOX4
Count
633nm 675/25 APC-NOX4
Mean Fl. % Pos.
EV 3,985 0.21
V5-NOX4 13,844 28.77
SB1-NOX4 17.916 42.14
NOX4-SB5 19,212 49.34
NOX4-SB6 10,982 20.72
F
NOX4
NOX4
extracellular
intracellular
p22
linker
linker
SB
LB
90°
linker
SB
LB
G
n.s.
Luminescence (RLU x 10⁶)
SB1-NOX4 + p22-LB2
NOX4-LB1 + p22-SB1
H
nmol H2O2/h/mg protein
EV
SB1-NOX4 + p22-LB2
NOX4-LB1 + p22-SB1
I
NOX4
p22phox
Actin
100kDa
70kDa
55kDa
35kDa
25kDa
45kDa
EV
SB1-NOX4 + p22-LB2
NOX4-LB1 + p22-SB1
J
Count
633 675/25 APC-NOX4
% Pos.
EV 0.55±0.1
SB1-NOX4 35.3±4.0
NOX4-LB1 37.0±2.7
K
Luminescence (RLU x10⁶)
SB1 LB2
LB2 SB1
LB2 131SB
LB2 172SB
NOX4 p22
L
nmol H2O2/h/mg protein
EV
SB1 LB2
LB2 SB1
LB2 131SB
LB2 172SB
NOX4 p22

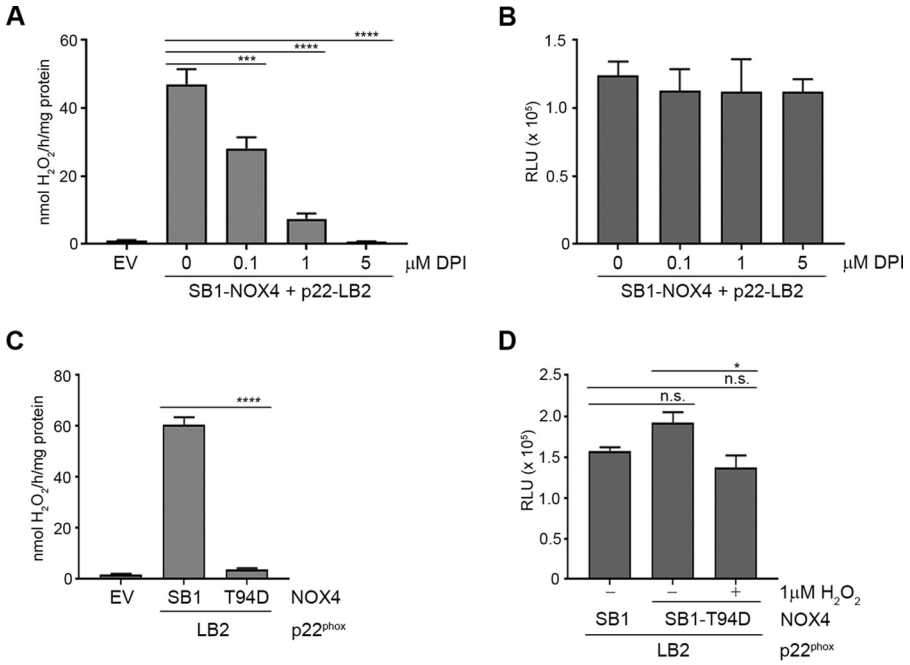

Figure 3. Reactive oxygen species do not alter the NanoBiT interaction or NanoLuc readout. *A*, DPI inhibits catalytic activity (H_2O_2 release) of SB1-NOX4/p22-LB2. *B*, DPI does not alter the luminescence signal of SB1-NOX4/p22-LB2. *C*, H_2O_2 release of NOX4 WT *versus* catalytically inactive SB1-NOX4 T94D mutant. *D*, luminescence signal after exogenously supplementing H_2O_2 to indicated NOX4 complexes. Statistical analysis in *A*, *B*, and *D* was performed using a one-way ANOVA with post hoc Tukey's multiple-comparison test and in *C* by using an unpaired, two-tailed Student's *t* test. *Error bars*, S.E. *n.s.*, not significant; *, $p \leq 0.05$; ***, $p \leq 0.001$; ****, $p \leq 0.001$.

plex was properly formed but did not provide the appropriate distance for SB/LB interaction, as SB5 is localized on the opposite side in the folded model (Fig. 2*F*, SB5 surface *red*). This observation reveals the critical importance of a multipronged approach when designing and validating interaction pairs. Comparison of NOX4-SB5 with the adjacent NOX4-SB6 identified a novel and unique region in the NOX4 C terminus that can be structurally modified without altering enzyme activity. Docking of the NanoLuc structure (PDB entry 5IBO) to the SB1-NOX4/p22-LB2 model indicates an approximate distance of 40 Å between the NOX4 N terminus and the $p22^{phox}$ C terminus, necessitating long linkers to accommodate the shorter 25-Å distance between the SB and LB termini. The model suggests that C-terminal fusions, such as the combination NOX4-LB1/p22-SB1, will form a complex. This interaction was confirmed, albeit, as expected from the earlier GFP studies (Fig. 1), with markedly reduced catalytic activity, although protein expression and cell-surface localization were comparable with catalytically active SB1-NOX4/p22-LB2 (Fig. 2, *G–J*). In contrast to N-terminal GFP-NOX4 (7), introduction of LB at the NOX4 N terminus (LB2-NOX4/p22-SB1) resulted in significantly reduced PPI and H_2O_2 generation (Fig. 2, *K* and *L*), indicating that SB *versus* LB orientation and linker length as well as the choice of fusion protein are critical aspects for NanoBiT association and NOX4 activity.

The NOX4-$p22^{phox}$ PPI may serve as a high-throughput screening assay

High-throughput screening for small molecule modulators targeting PPI interfaces can identify lead compounds with increased selectivity for disrupting signaling circuits (13). Existing NOX inhibitors are pan-flavoenzyme inhibitors or radical scavengers or NOX inhibitors lacking isoform selectivity. We reported that complex formation between NOX4 and $p22^{phox}$ differs from other NOX isoforms (7), opening the door for selective PPI inhibitors. In the case of constitutively active NOX4, enzyme activity could alter PPI readout by oxidation (overexpression output 30–100 nmol of H_2O_2/h/10^6 cells). However, the SB1-NOX4/p22-LB2 luminescence signal was not affected by released or exogenously supplemented H_2O_2 (Fig. 3). After miniaturization to 1536-well format, selected compounds currently used as NOX inhibitors were tested in the NOX4 PPI assay. As expected, diphenyleneiodonium (DPI), which targets flavin via irreversible phenylation (14), or GKT compounds, which can inhibit NOX1–4 (15), but also $p22^{phox}$-independent NOX5 and DUOX enzymes (16, 17), did not alter PPI (Fig. S3). Some compounds reduced at high concentrations the luminescence signal of the NOX4/$p22^{phox}$ PPI but decreased then also the signal generated by an unrelated PPI pair or by the cell-free NanoLuc substrate control. Thus, cer-

Figure 2. Development of a PPI assay for the NOX4-$p22^{phox}$ complex combined with functional analysis. *A*, topological scheme of the NOX4/$p22^{phox}$ complex with selected interaction pairs. *B* and *G*, determination of PPI by NanoLuc luminescence (RLU percentage of control). *C* and *H*, catalytic activity (H_2O_2 release). *D* and *I*, protein expression (immunoblotting). *E* and *J*, cell-surface localization using anti-NOX4 antibody to an extracellular domain. *F*, NOX4-$p22^{phox}$ homology model in surface presentation depicting location of NanoBiT assembly in a *cartoon representation* (SB1-NOX4/p22-LB2; *red arrow* indicates SB5 location). *K* and *L*, PPI (luminescence) and H_2O_2 generation of SB *versus* LB N-terminally tagged NOX4 matched with full-length *versus* truncated $p22^{phox}$. *Error bars*, S.E. Analysis for *G* and *H* was an unpaired, two-tailed Student's *t* test; *B*, *C*, *K*, and *L*, one-way ANOVA with post hoc Tukey's multiple-comparison test. *n.s.*, not significant; **, $p \leq 0.01$; ***, $p \leq 0.001$; ****, $p \leq 0.001$.

tain compounds used as nonspecific NOX inhibitors (at up to 50 μM) caused a higher false positive hit rate in the NanoBiT assay than reported previously for a LOPAC^{1280} library (10 μM) (18), emphasizing the need for robust counterscreens.

Integrated analysis of NOX4 and CYBA mutations identifies PPI hot spot residues

Naturally occurring or induced missense mutations constitute an ideal tool for PPI validation and the mapping of heterodimer interfaces. Introduction of mutations that affect NOX4 cytosolic domains and are primarily connected to NOX catalytic activity, such as T94D (NOX4-specific B-loop) (10), P437H (conserved $NADPH_1$-binding site), or R523D (conserved GRP sequence), did not alter PPI (Fig. 4, *A* and *B*). Heterodimerization was also not affected in SB1-NOX4$^{H222Q/C226V}$, a double mutation in the second extracellular loop (E-loop) (Fig. 4*B*), yet this mutant failed to translocate in the majority of cells (Fig. 4, *E* and *F*). In HEK293 cells, which retain the majority of NOX4 on intracellular membranes and cannot be used for trafficking analysis, single H222Q and C226V mutations generated intracellular superoxide instead of H_2O_2 (19). We show here that replacing certain E-loop residues located close to TMH5 impairs trafficking of the assembled heterodimer, which could be due to reduced binding to ER chaperones, such as calnexin (20). Mutation of histidines serving as heme ligands in TMH3 and TMH5 (H119L and H119L/H194L) rendered NOX4 catalytically inactive and reduced PPI significantly (Fig. 4, *A–D*). In accord, treatment of SB1-NOX4/p22-LB2–expressing cells with the heme synthesis inhibitor succinyl acetone reduced luminescence and H_2O_2 generation (not shown). These results indicate that NOX4 follows the NOX2 paradigm, where heme incorporation is a prerequisite for heterodimerization (21). Nonstabilized NOX4 His-119 and His-119/194 mutants failed to translocate to the plasma membrane (Fig. 4, *E* and *F*).

Missense variants in *CYBA* (p22^{phox}) cause the immunodeficiency disorder chronic granulomatous disease due to defective assembly of the multimeric NOX2 complex. In A22^0 chronic granulomatous disease patients, *CYBA* variants lead to loss of both p22^{phox} and NOX2 protein, as heterodimerization is required for the stability of both proteins in neutrophils (22). These rare *CYBA* variants may affect all NOX family members that rely on p22^{phox} as a dimerization partner (NOX1–4). Because the CYBA p.Gly24Arg variant in TMH1 is rather common (http://structure.bmc.lu.se/idbase/CYBAbase) (48),[5] it was introduced into p22-LB2 and co-expressed with SB1-NOX4. H_2O_2 production and heterodimerization were significantly reduced, and ~50% of the SB1-NOX4/p22-LB2^{G24R} complex was trapped in the ER in epithelial cells (Fig. 5, *A–E*). Mutant p22^{phox} mice (*Cyba^{nmf333}*, p22^{phox} Y121H) display a Nox2 and Nox3 loss-of-function phenotype (23), whereas NOX4 activity is not affected by this mutation (7), suggesting increased structural flexibility of the NOX4/p22^{phox} complex and/or differences in the interaction surface with p22^{phox}. SB-LB tagging slightly reduced luminescence and H_2O_2 production of SB1-NOX4/p22-LB^{Y121H} (20–25%), but the majority of NOX4 translocated to the cell surface (Fig. 5, *A–E*). Inducing a β turn in TMH4 by replacing Tyr-121 with proline (p22^{phox} Y121P) is predicted to disrupt the complex. In accord, heterodimerization, catalytic activity, and cell-surface expression of SB1-NOX4/p22-LB2^{Y121P} were markedly reduced. A close-up of the NOX4-p22^{phox} interface shows that p22^{phox} forms an extensive network of hydrophobic interactions with NOX4 via Leu–Leu and Leu–Val contacts. The clustering of numerous hydrophobic contacts at the heterodimer interface will create a leucine zipper-like structure. Owing to the position of Tyr-121 in the last p22^{phox} TMH, a proline substitution will alter the helix structure by breaking hydrophobic contacts and the hydrogen bond between NOX4 Ile-182 and p22^{phox} Thr-64 (Fig. 5*F*). Arg-90 in p22^{phox} forms a hydrogen bond with the p22^{phox} Gly-24 backbone residue and NOX4 Thr-163. Thus, mutation of Gly-24 to arginine will destabilize both the p22^{phox} fold due to repulsive charge and the hydrophobic interaction network between p22^{phox} and NOX4 (Fig. 5*F*). Hence, the p22^{phox} TMH4 penultimate amino acid residues discriminate between NOX isoforms and affect selectively heterodimerization with p22^{phox}, whereas changes in the p22^{phox} Gly-24 region (TMH1) influence heterodimerization with NOX4, NOX2, and probably NOX1/3.

Discussion

NADPH oxidases constitute a prime drug target for the treatment of diseases associated with chronic superoxide/H_2O_2 overproduction, such as fibrotic, cardiovascular, or metabolic diseases (16). Almost all currently available small molecule inhibitors are not NOX isoform–selective and will interfere with redox signaling in a nonspecific manner. Inhibitors of the NOX electron transport chain are usually nonspecific due to high identity or homology of the involved domains and amino acid residues, although a NOX2-selective, NADPH-competitive compound was described recently (24). Therapeutic disruption of the NOX membrane protein complex could lead to isoform selective compounds but is difficult to achieve, as the structure of the complex remains unresolved. A partial structure of a NOX5 homolog expressed in the cyanobacterium *Cylindrospermum stagnale* has been reported (25), but NOX5-type oxidases differ substantially from NOX1–4 and DUOX1–2 enzymes, as heterodimerization is not required. Using knowledge accumulated by NOX protein engineering, disease-associated missense mutations, and NOX complex modeling, we developed a NOX4/p22^{phox} PPI assay that distinguished between catalytic *versus* structural alterations, identified two hot spots in p22^{phox} (TMH1 and TMH4), and revealed NOX4 loop involvement (loops D and E) in complex formation and/or trafficking. Hence, this PPI assay will not only support a deeper understanding of the catalytic center of the NOX4 enzyme, but can also assist in functional analysis of human disease-associated variants. Development of this assay expands our repertoire for assessing protein–protein interactions, as until now immunoprecipitation of NOX or p22^{phox} from detergent-containing extracts was the only means for analyzing complex formation. Immunoprecipitation depends on the antibody selectivity and affinity, is highly variable, and is not quantitative.

[5] Please note that the JBC is not responsible for the long-term archiving and maintenance of this site or any other third party hosted site.

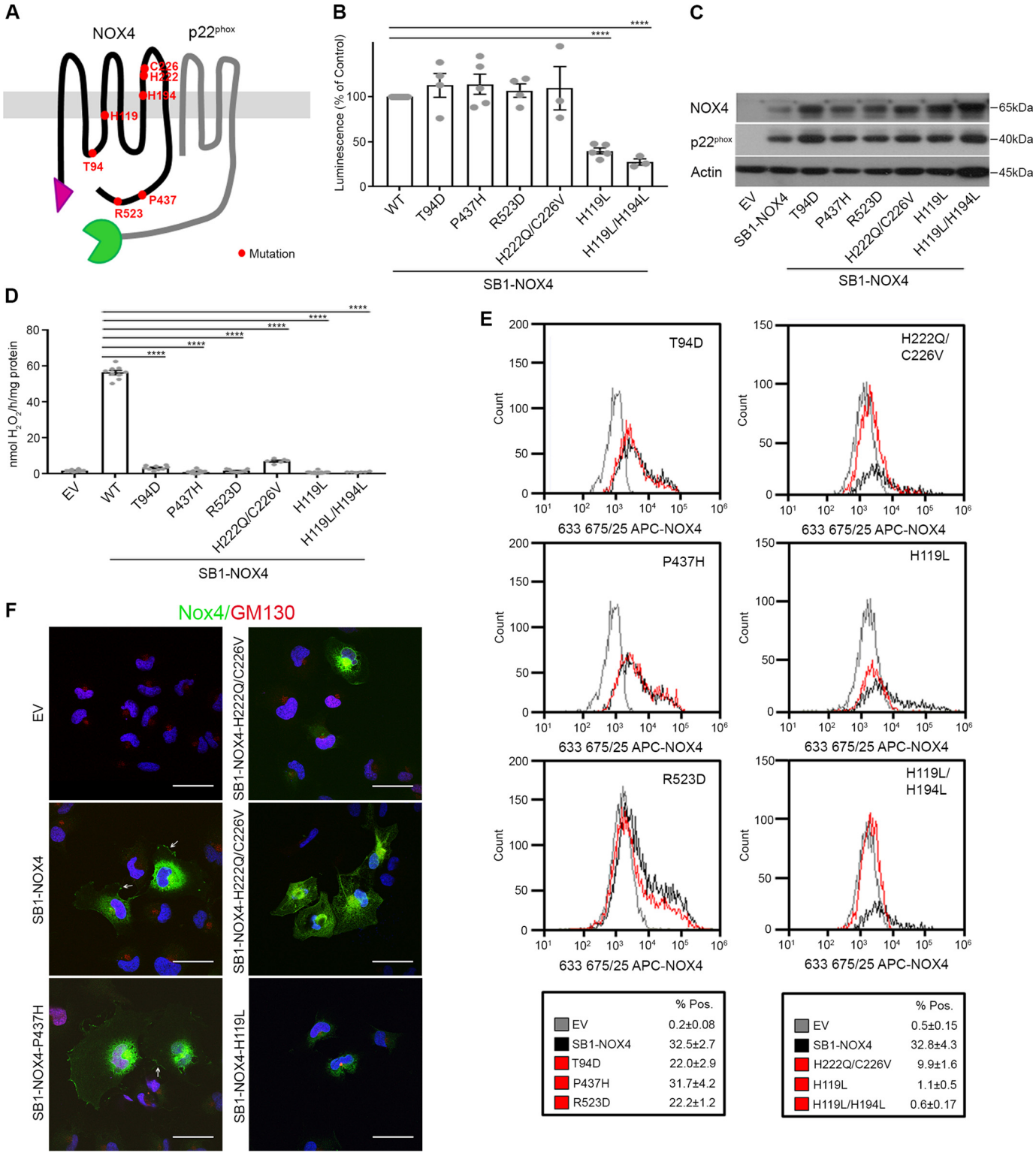

Figure 4. PPI analysis of NOX4 mutants. *A*, scheme of selected NOX4 mutations. *B–F*, luminescence (PPI), protein expression, H_2O_2 generation, flow cytometry, and immunofluorescence of SB1-NOX4 mutants defective in catalytic activity or heme incorporation, paired with p22-LB2. *Error bars*, S.E. Analysis for *B* and *D* was one-way ANOVA with post hoc Tukey's multiple-comparison test. ****, $p \leq 0.001$.

By permitting quantitative monitoring of conformational dimerization, the PPI assay constitutes also a novel tool for multiplexed high-throughput screening to identify candidate NOX inhibitors targeting either complex assembly or complex disruption or inducing allosteric modulation. The minimal steric burden inherent in this reversible, sensitive PPI system conveys a distinct advantage for intricate complex assemblies with multiple sensitive structural features. Our preliminary test of this NOX4 PPI assay indicates that current compounds used to inhibit NADPH oxidases do not target NOX4-p22^{phox} het-

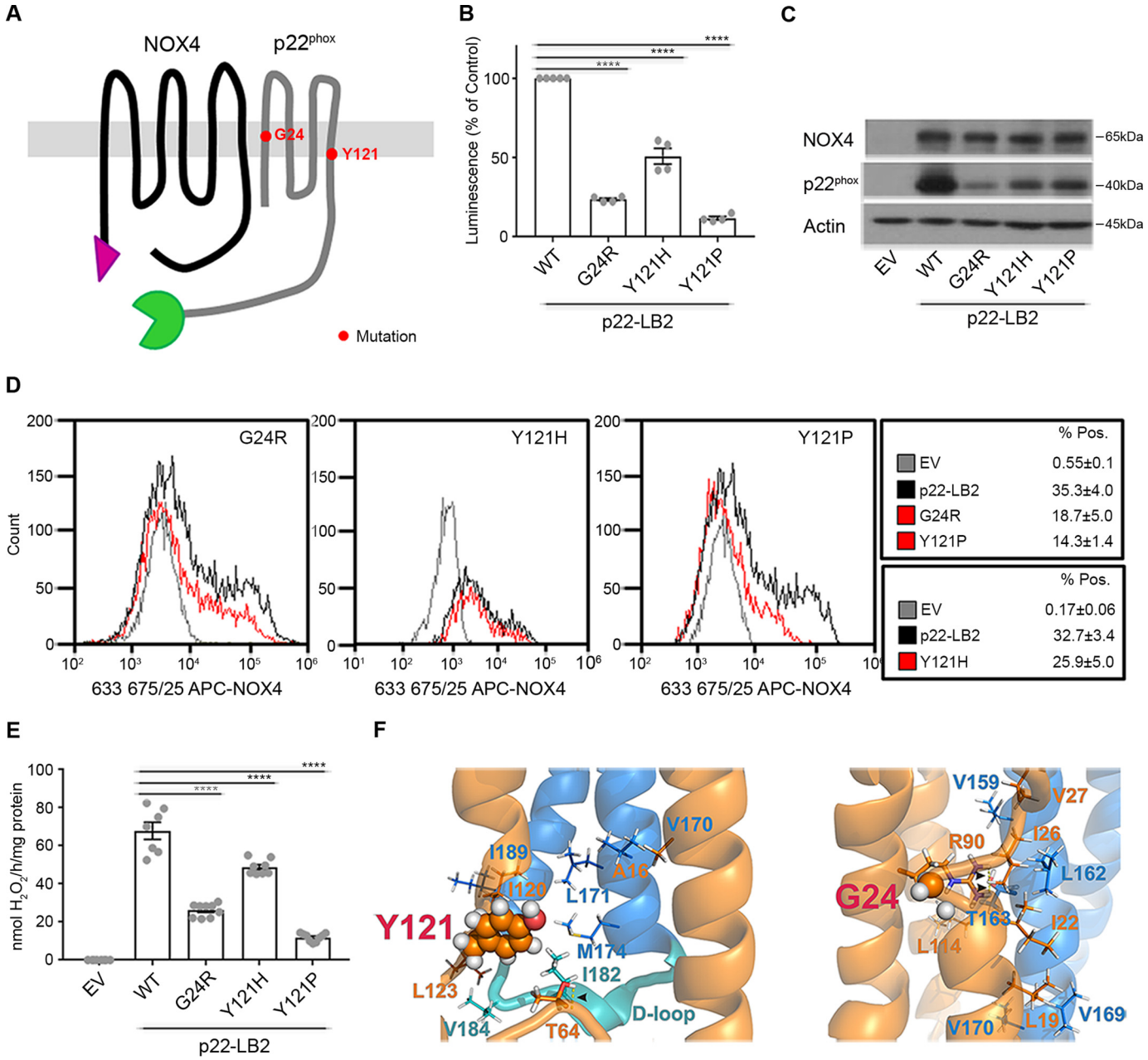

Figure 5. PPI analysis of p22^{phox} mutants. *A*, scheme of selected p22^{phox} mutations. *B–E*, luminescence (PPI), protein expression, flow cytometry, and H_2O_2 generation of p22-LB2 TMH mutants paired with SB1-NOX4. *F*, heterodimer model showing interaction of p22^{phox} residues in TMH1 and TMH4 (Gly-24) or TMH1, TMH3, and TMH4 (Tyr-121) with NOX4 residues (*spheres* represent p22^{phox} Tyr-121 and Gly-24, *sticks* represent residues forming hydrogen bonds, *lines* represent residues forming hydrophobic interactions). *Error bars*, S.E. Analysis for *B* and *E* was one-way ANOVA with post hoc Tukey's multiple-comparison test. ****, $p \leq 0.001$.

erodimerization. The utility of this PPI for NOX4 inhibitor discovery can be improved by inducible stable incorporation of the PPI pair into NOX4/p22^{phox}-deficient cells. Establishing similar assays for other NOX isoforms may reveal additional determinants for assembly, improve prediction of human disease variant effects, and further support development of NOX isoform–selective PPI drug candidates. Requiring only a minimal-size fusion tag on one of the protein interaction partners was critical for maintaining a catalytically active, properly assembled oxidase enzyme. Although not tolerated by NOX4, insertion of the small split fragment into loop or surface regions of multipass membrane proteins will provide a distinct advantage for real-time association studies in cells. This approach will probably be enabling for structure–function studies and drug discovery platforms of a wide variety of membrane protein complexes of unknown structure.

Experimental procedures

Plasmid construction

Human NOX4(1–578) (NM_016931.3) and p22^{phox}(1–195, 1–172, and 1–131) (NM_000101.3) WT and featuring SB/LB additions/insertions and various linkers were cloned into pcDNA3.1 (not in Promega pNBe vectors). SB1-NOX4 (SB-GS linker-V5-V5-NOX4(2–578)), SB2-NOX4 (SB-GS linker-V5-NOX4(2–578)), NOX4-SB3 (NOX4-A177-SB-I189-NOX4),

NOX4-SB4 (NOX4-A177-GS linker-SB-GS linker-I189-NOX4), NOX4-SB5 (NOX4-P388-SB-Q400-NOX4), NOX4-SB6 (NOX4-F398-SB-D410-NOX4), NOX4-SB7 (NOX4-I508-SB-F520-NOX4), NOX4-SB8 (NOX4-I508-GS linker-SB-GS linker-F520-NOX4), NOX4-SB9 (NOX4-Δ575–578-GS linker-SB), NOX4-LB1 (NOX4-Δ575–578-GS linker-LB), LB2-NOX4 (LB-GS linker-V5-V5-NOX4), p22-SB1 (p22-GS linker-SB), p22-LB1 (p22-alanine linker-LB), p22-LB2 (p22-GS linker-LB), p22–131SB (p22(1–131)-GS linker-SB), p22–131LB (p22(1–131)-GS linker-LB), p22–172SB (p22(1–172)-GS linker-SB), p22–172LB (p22(1–172)-GS linker-LB). GS (sequence GSSGGGGSGGGGSSG and multiple variations, 4–30 aa) and AA linkers (5 aa) were used; when compared, the linker length did not substantially alter the performance of the SB-LB interaction pairs. Point mutants SB1-NOX4 (T94D, P437H, R523D, H222Q/C226V, H119L, and H119L/H194L) and p22-LB2 (G24R, Y121H, and Y121P) were generated by PCR site-directed mutagenesis and verified by sequencing. Mutations were also introduced into pcDNA3.1-NOX4 WT, pcDNA3.1-V5-V5-NOX4, or pcDNA3.1-p22^{phox} WT. NOX4 was also cloned into pEGFP-C1 (28-aa linker) and pEGFP-N1 (8-aa linker).

Cell culture and transfection

NOX/DUOX-deficient COS7 cells stably expressing p22^{phox} (26) were maintained in Dulbecco's modified Eagle's medium with 10% fetal bovine serum. Most experiments were performed with NOX/DUOX/p22^{phox}-deficient NCI-H661 cells maintained in RPMI 1640 medium with 10% fetal bovine serum. Transient transfections of H661 and COS-p22^{phox} cells were performed using Dreamfect Gold (Oz Biosciences) or Lipofectamine 3000 (Invitrogen) according to the manufacturers' instructions. Briefly, cells were plated at a density of 5×10^4 cells/well in a 12-well plate and transfected with a total of 375 ng of DNA (2:1 ratio of NOX4/p22^{phox} DNA) per well for 48 h. Medium was changed the day after transfection.

Protein isolation and Western blotting

Cells were lysed in ice-cold radioimmune precipitation assay lysis buffer, and cleared lysates, after electrophoresis and blotting, were probed with antibodies directed to NOX4 (clone 20.3, epitope and validation as in Ref. 7), p22^{phox} (FL-195, Santa Cruz Biotechnology, Inc.; 16G7 (27)), GFP (NB600-308ss, Novus), and actin (A2066, Sigma). Secondary antibodies were horseradish peroxidase–conjugated anti-mouse (Cell Signaling) or anti-rabbit antibodies (Southern Biotech). Protein bands were detected using ECL reagent (Pierce).

Measurement of H_2O_2 production

H_2O_2 release was measured by monitoring homovanillic acid (HVA) fluorescence as described previously (4). Briefly, cells were washed in PBS with Ca^{2+} and Mg^{2+} and incubated at 37 °C for 1 h in HVA solution (100 mM HVA, 4 units/ml horseradish peroxidase in PBS with Ca^{2+} and Mg^{2+}). The reaction was terminated by the addition of Stop buffer (0.1 M glycine, 0.1 M NaOH, pH 12, and 25 mM EDTA in PBS). Fluorescence was read on a Biotek Synergy HT plate reader (320-nm excitation, 420-nm emission). Fluorescence readings were converted into nmol of H_2O_2 based on a H_2O_2 standard curve and normalized to cell lysate protein content.

Luciferase assay for protein–protein interactions

The Nano-Glo® live cell assay kit (Promega) was used as follows. Cells were seeded at 7.5×10^3 cells/well in a white, clear-bottom 96-well plate 24 h before transfection (10 ng each of NOX4 and p22^{phox}, combined with 480 ng of pBluescript DNA). After 48-h transfection, medium was removed and replaced with 100 μl of Opti-MEM medium for 1 h at 37 °C. The Nano-Glo® reagent was prepared as per the manufacturer's instructions and added to each well immediately before the luminescence reading was taken. Luminescence was measured at 10–20-s intervals for 15 min on a Berthold Centro 960 LB and reported as relative light units (RLU). For quantitative comparison of SB-LB interactions, the peak values at the 2–3-min time point were used.

Flow cytometry

H661 cells expressing the pair SB1-NOX4 and p22-LB2 or other combinations/mutations, as indicated, were incubated on ice with anti-NOX4 antibody in FACS buffer (PBS with Mg^{2+}/Ca^{2+}, 5% BSA) for 30 min without permeabilization. After incubation with anti-rabbit allophycocyanin (Invitrogen), cells were fixed with 1.5% paraformaldehyde and analyzed on an Accuri C6 flow cytometer (BD Biosciences).

Fluorescence microscopy

H661 cells were seeded at 2.5×10^4 cells/well on poly-L-lysine–coated glass coverslips and transfected as described. Cells were fixed in 3% paraformaldehyde, followed by permeabilization with 0.1% Triton X-100 and blocking in PBS containing 1.5% BSA and 3% goat serum. Cells were stained with antibodies directed to NOX4, calnexin (MAB3126, Chemicon), or GM130 (610822, BD Transduction Laboratories) antibodies. Secondary antibodies were goat anti-rabbit Alexa Fluor 488 and goat anti-mouse Alexa Fluor 647 (Thermo Fisher). Nuclear stain was obtained using DAPI (Sigma). Images were taken on an Olympus Fluoview FV1000 confocal microscope (Olympus) using a ×60 oil objective. Images were processed using ImageJ (version 1.48) and Photoshop CC.

Protein modeling, docking, and molecular dynamics simulation

A three-dimensional model of the SB1-NOX4/p22-LB2 complex was constructed in multiple steps. *Ab initio* NOX4 and p22^{phox} secondary structure prediction was performed using the ROSETTA-based Robetta webserver (28). The model of the transmembrane domains of NOX4 was generated using the homology modeling program Modeler 9v14 (29). To identify the most suitable templates, a BLAST search of PDB was performed with the NOX4(1–305) sequence and cyanobacterium *Cylindrospermum stagnale* Nox5 (PDB 5O0T), and four cytochrome *c* oxidoreductase complexes with the highest homology served as initial templates. The NOX4(1–305) sequence was aligned to the templates using Clustal (http://www.ebi.ac.uk/Tools/msa/clustalo/)[5] (49) and alignment was adjusted manually, taking into account the secondary structure prediction and previously published data (6, 7, 10, 30–34). Modeling was per-

formed with the default parameters using the "allHmodel" protocol to include hydrogen atoms, the "HETATM" protocol to include heme with restricting heme-binding histidine residue side-chain distance, and a thorough molecular dynamics MD optimization and refinement protocol. The secondary structure of each individual loop was further optimized using the "loopmodel" protocol (35). As per the procedure described above, the $p22^{phox}$(1–121) transmembrane domains were generated by combining previously available structural information and secondary structure prediction (7, 32, 36, 37). The transmembrane domain of NOX4 was docked to its cytosolic C-terminal NADPH/FAD binding domain (PDB entries 3A1F and 5O0T (38)) using HADDOCK (39, 40). Docking was performed with most of the parameters set to default using the web server version of HADDOCK with a Guru interface including heme, FAD, and NADPH in the docking run. Semiflexible segments and active residues were manually defined (transmembrane, FAD, or NADPH domain each represented as one segment), whereas passive residues were defined automatically. HADDOCK proposed only one probable cluster of similar models, and the model with the lowest Van der Waals, electrostatic, and desolvation energy was chosen. The chosen model also had the shortest FAD–heme distance. The transmembrane $p22^{phox}$ domains (4-TMH model for best fit) were then docked to NOX4 using HADDOCK, as described above. Using Modeler, the $p22^{phox}$ C terminus, SB1, and LB2 (PDB entry 5IBO) were added, and its folding was simulated using a NAMD 2.11 (http://www.ks.uiuc.edu/Research/namd/)[5] (50) plug-in in the VMD version 1.9.2.27 program (http://www.ks.uiuc.edu/Research/vmd/)[5] (51) for 10 ms. Intermediate and final structures were evaluated in PyMOL.

Testing of compounds in a miniaturized plate format

The transfection protocol described below is the result of optimization of multiple parameters, including cell number to transfect and response to linearity, DNA *versus* Lipofectamine ratio, duration of protein expression, assay tolerance to DMSO, and statistical quality (*Z* value).

Transient transfection of SB1-NOX4/p22-LB2 pairs—NCI-H661 cells were maintained using RPMI 1640 medium (Thermo Fisher Scientific) with 10% fetal bovine serum (Bioconcept, Allschwil, Switzerland). All cell cultures were maintained inside a humidified incubator at 37 °C and 5% CO_2. Transfection using Lipofectamine® 3000 (Thermo Fisher Scientific) was performed according to the manufacturer's protocol with a DNA/Lipofectamine ratio of 1:2.22 (w/v). A transfection enhancer, the 3000 enhancer reagent (1:2 DNA/reagent (w/v)), was used along with the Lipofectamine® 3000 transfection reagent for all transfections. Transfection reagents were diluted in Opti-MEM™ (Thermo Fisher Scientific) and added to the cell suspension before cell distribution to a 1536-w plate with black walls and transparent bottom, tissue culture–treated (792091-191, Greiner bio-one, St. Gallen, Switzerland). Typically 3 ng of plasmid DNA for 500 cells per 4 μl were transferred to each well of the 1536-well plate (with a 1:1 ratio of SB1-NOX4/p22-LB2 (w/w)). The transfection protocol for KRAS-LB/cRAF G12C-SB is identical to the one used for SB1-NOX4/p22-LB2.

Nano-Glo® assay—Detection of NanoLuc® Luciferase was performed following the manufacturer's protocol (Live Cell Method, Promega, Madison, WI). Compounds were tested by using a "disruptive mode" protocol. In these experiments, compounds are evaluated for their ability to disrupt an already formed complex following expression of NOX4 and $p22^{phox}$ pairs. To this end, cells were washed with HBSS containing 20 mM Hepes (pH 7.4) 20–24 h after cell transfection and incubated in 2 μl of HBSS containing 20 mM Hepes (pH 7.4). 40 nl of compounds in serial concentrations (Novartis Compound archive as 10 mM solutions in 100% DMSO or from powders diluted in 90% DMSO/water (v/v) diluted in 100% DMSO) were then added using an acoustic dispenser (Echo550, Labcyte Inc., Sunnyvale, CA) and incubated for another 1 h at 37 °C in a humidified atmosphere with 5% CO_2. The assay is very tolerant to DMSO, as this solvent could be used up to a 2.7% (v/v) final concentration without any negative impact on the signal amplitude. After incubation, plates were equilibrated at room temperature for 5–10 min. NanoLuc activity was detected by adding 2 μl of furimazine (NanoLuciferase substrate, a coelenterazine derivative) diluted in the buffer provided by the manufacturer or in PBS (final dilution of 1:100 in the well). Luminescence was measured for 10 s on an FDSS700 kinetic reader with 1-s integration times. Data are expressed as average luminescence counts over 10 s of four replicate wells.

Cell-free Nano-Glo® assay—Compounds were tested by replacing cells with 10 nM His_6-NanoLuc enzyme (903479, Promega, Madison, WI) diluted in PBS (2 μl/well). Luminescence was measured following a 1-h incubation.

NOX inhibitors

The following inhibitors were used: DPI, GKT137831 (41), GKT136901 and GKT compound 88 (42), apocynin (43, 44), ML171 (45), ebselen, VAS2870 (16), flavonoid compound 7h (46), and celastrol (47).

Statistical analysis

All experiments were performed at least three times in triplicate (the *error bars* indicate mean ± S.E., $n \geq 3$). Graphs for NanoBiT interaction assays are representative examples of at least three independent experiments. Bar graphs for NanoBiT interaction assays represent the RLU values obtained at the 2–3-min time point and include at least three separate experiments. For comparison of cell-based assays with transiently expressed mutants, the internal SB1-NOX4/p22-LB2 control was set to 100% for quantification. When indicated, a one-way ANOVA with post hoc Tukey's multiple-comparison test was performed. Statistical significance is indicated on the *bar graphs*: *n.s.*, not significant; *, $p \leq 0.05$; **, $p \leq 0.01$; ***, $p \leq 0.001$; ****, $p \leq 0.001$, comparing samples as indicated.

Author contributions—S. O. performed all functional assays, M. M. established PPI miniaturization and compound testing, S. Z. carried out cloning and mutagenesis, L. K. prepared the extended homology model and designed with UGK interaction pairs, D. S. participated in imaging analysis, and J. R. contributed to tool design. U. G. K., R. B., and U. S. developed the concept. U. G. K. directed the work, which was written with contributions from all authors.

Acknowledgments—We thank P. Hayes, C. Dahlem, and K. O'Neill for experimental assistance and Promega Corp. for providing NanoBiT reagents for beta testing.

References

1. Stynen, B., Tournu, H., Tavernier, J., and Van Dijck, P. (2012) Diversity in genetic *in vivo* methods for protein–protein interaction studies: from the yeast two-hybrid system to the mammalian split-luciferase system. *Microbiol. Mol. Biol. Rev.* **76,** 331–382 CrossRef Medline
2. Dixon, A. S., Schwinn, M. K., Hall, M. P., Zimmerman, K., Otto, P., Lubben, T. H., Butler, B. L., Binkowski, B. F., Machleidt, T., Kirkland, T. A., Wood, M. G., Eggers, C. T., Encell, L. P., and Wood, K. V. (2016) NanoLuc complementation reporter optimized for accurate measurement of protein interactions in cells. *ACS Chem. Biol.* **11,** 400–408 CrossRef Medline
3. Luxen, S., Noack, D., Frausto, M., Davanture, S., Torbett, B. E., and Knaus, U. G. (2009) Heterodimerization controls localization of Duox-DuoxA NADPH oxidases in airway cells. *J. Cell Sci.* **122,** 1238–1247 CrossRef Medline
4. Martyn, K. D., Frederick, L. M., von Loehneysen, K., Dinauer, M. C., and Knaus, U. G. (2006) Functional analysis of Nox4 reveals unique characteristics compared to other NADPH oxidases. *Cell. Signal.* **18,** 69–82 CrossRef Medline
5. Hecker, L., and Thannickal, V. J. (2016) Getting to the core of fibrosis: targeting redox imbalance in aging. *Ann. Transl. Med.* **4,** 93 CrossRef Medline
6. von Löhneysen, K., Noack, D., Wood, M. R., Friedman, J. S., and Knaus, U. G. (2010) Structural insights into Nox4 and Nox2: motifs involved in function and cellular localization. *Mol. Cell. Biol.* **30,** 961–975 CrossRef Medline
7. von Löhneysen, K., Noack, D., Jesaitis, A. J., Dinauer, M. C., and Knaus, U. G. (2008) Mutational analysis reveals distinct features of the Nox4-p22 phox complex. *J. Biol. Chem.* **283,** 35273–35282 CrossRef Medline
8. Casbon, A. J., Allen, L. A., Dunn, K. W., and Dinauer, M. C. (2009) Macrophage NADPH oxidase flavocytochrome B localizes to the plasma membrane and Rab11-positive recycling endosomes. *J. Immunol.* **182,** 2325–2339 CrossRef Medline
9. Ambasta, R. K., Kumar, P., Griendling, K. K., Schmidt, H. H., Busse, R., and Brandes, R. P. (2004) Direct interaction of the novel Nox proteins with p22phox is required for the formation of a functionally active NADPH oxidase. *J. Biol. Chem.* **279,** 45935–45941 CrossRef Medline
10. von Löhneysen, K., Noack, D., Hayes, P., Friedman, J. S., and Knaus, U. G. (2012) Constitutive NADPH oxidase 4 activity resides in the composition of the B-loop and the penultimate C terminus. *J. Biol. Chem.* **287,** 8737–8745 CrossRef Medline
11. Jackson, H. M., Kawahara, T., Nisimoto, Y., Smith, S. M., and Lambeth, J. D. (2010) Nox4 B-loop creates an interface between the transmembrane and dehydrogenase domains. *J. Biol. Chem.* **285,** 10281–10290 CrossRef Medline
12. Zhen, L., Yu, L., and Dinauer, M. C. (1998) Probing the role of the carboxyl terminus of the gp91phox subunit of neutrophil flavocytochrome b558 using site-directed mutagenesis. *J. Biol. Chem.* **273,** 6575–6581 CrossRef Medline
13. Scott, D. E., Bayly, A. R., Abell, C., and Skidmore, J. (2016) Small molecules, big targets: drug discovery faces the protein-protein interaction challenge. *Nat. Rev. Drug Discov.* **15,** 533–550 CrossRef Medline
14. O'Donnell, B. V., Tew, D. G., Jones, O. T., and England, P. J. (1993) Studies on the inhibitory mechanism of iodonium compounds with special reference to neutrophil NADPH oxidase. *Biochem. J.* **290**, 41–49 CrossRef Medline
15. Gaggini, F., Laleu, B., Orchard, M., Fioraso-Cartier, L., Cagnon, L., Houngninou-Molango, S., Gradia, A., Duboux, G., Merlot, C., Heitz, F., Szyndralewiez, C., and Page, P. (2011) Design, synthesis and biological activity of original pyrazolo-pyrido-diazepine, -pyrazine and -oxazine dione derivatives as novel dual Nox4/Nox1 inhibitors. *Bioorg. Med. Chem.* **19,** 6989–6999 CrossRef Medline
16. Altenhöfer, S., Radermacher, K. A., Kleikers, P. W., Wingler, K., and Schmidt, H. H. (2015) Evolution of NADPH oxidase inhibitors: selectivity and mechanisms for target engagement. *Antioxid. Redox Signal.* **23,** 406–427 CrossRef Medline
17. Strengert, M., Jennings, R., Davanture, S., Hayes, P., Gabriel, G., and Knaus, U. G. (2014) Mucosal reactive oxygen species are required for antiviral response: role of Duox in influenza A virus infection. *Antioxid. Redox Signal.* **20,** 2695–2709 CrossRef Medline
18. Hall, M. P., Unch, J., Binkowski, B. F., Valley, M. P., Butler, B. L., Wood, M. G., Otto, P., Zimmerman, K., Vidugiris, G., Machleidt, T., Robers, M. B., Benink, H. A., Eggers, C. T., Slater, M. R., Meisenheimer, P. L., *et al.* (2012) Engineered luciferase reporter from a deep sea shrimp utilizing a novel imidazopyrazinone substrate. *ACS Chem. Biol.* **7,** 1848–1857 CrossRef Medline
19. Takac, I., Schröder, K., Zhang, L., Lardy, B., Anilkumar, N., Lambeth, J. D., Shah, A. M., Morel, F., and Brandes, R. P. (2011) The E-loop is involved in hydrogen peroxide formation by the NADPH oxidase Nox4. *J. Biol. Chem.* **286,** 13304–13313 CrossRef Medline
20. Prior, K. K., Wittig, I., Leisegang, M. S., Groenendyk, J., Weissmann, N., Michalak, M., Jansen-Dürr, P., Shah, A. M., and Brandes, R. P. (2016) The endoplasmic reticulum chaperone calnexin is a NADPH oxidase NOX4 interacting protein. *J. Biol. Chem.* **291,** 7045–7059 CrossRef Medline
21. DeLeo, F. R., Burritt, J. B., Yu, L., Jesaitis, A. J., Dinauer, M. C., and Nauseef, W. M. (2000) Processing and maturation of flavocytochrome b_{558} include incorporation of heme as a prerequisite for heterodimer assembly. *J. Biol. Chem.* **275,** 13986–13993 CrossRef Medline
22. van den Berg, J. M., van Koppen, E., Ahlin, A., Belohradsky, B. H., Bernatowska, E., Corbeel, L., Español, T., Fischer, A., Kurenko-Deptuch, M., Mouy, R., Petropoulou, T., Roesler, J., Seger, R., Stasia, M. J., Valerius, N. H., *et al.* (2009) Chronic granulomatous disease: the European experience. *PLoS One* **4,** e5234 CrossRef Medline
23. Nakano, Y., Longo-Guess, C. M., Bergstrom, D. E., Nauseef, W. M., Jones, S. M., and Bánfi, B. (2008) Mutation of the Cyba gene encoding p22 causes vestibular and immune defects in mice. *J. Clin. Invest.* **118,** 1176–1185 Medline
24. Hirano, K., Chen, W. S., Chueng, A. L., Dunne, A. A., Seredenina, T., Filippova, A., Ramachandran, S., Bridges, A., Chaudry, L., Pettman, G., Allan, C., Duncan, S., Lee, K. C., Lim, J., Ma, M. T., *et al.* (2015) Discovery of GSK2795039, a novel small molecule NADPH oxidase 2 inhibitor. *Antioxid. Redox Signal.* **23,** 358–374 CrossRef Medline
25. Magnani, F., Nenci, S., Millana Fananas, E., Ceccon, M., Romero, E., Fraaije, M. W., and Mattevi, A. (2017) Crystal structures and atomic model of NADPH oxidase. *Proc. Natl. Acad. Sci. U.S.A.* **114,** 6764–6769 Medline
26. Price, M. O., McPhail, L. C., Lambeth, J. D., Han, C. H., Knaus, U. G., and Dinauer, M. C. (2002) Creation of a genetic system for analysis of the phagocyte respiratory burst: high-level reconstitution of the NADPH oxidase in a nonhematopoietic system. *Blood* **99,** 2653–2661 CrossRef Medline
27. Campion, Y., Jesaitis, A. J., Nguyen, M. V., Grichine, A., Herenger, Y., Baillet, A., Berthier, S., Morel, F., and Paclet, M. H. (2009) New p22-phox monoclonal antibodies: identification of a conformational probe for cytochrome b_{558}. *J. Innate Immun.* **1,** 556–569 CrossRef Medline
28. Kim, D. E., Chivian, D., and Baker, D. (2004) Protein structure prediction and analysis using the Robetta server. *Nucleic Acids Res.* **32,** W526–W531 CrossRef Medline
29. Sali, A., and Blundell, T. L. (1993) Comparative protein modelling by satisfaction of spatial restraints. *J. Mol. Biol.* **234,** 779–815 CrossRef Medline
30. Kawahara, T., Quinn, M. T., and Lambeth, J. D. (2007) Molecular evolution of the reactive oxygen-generating NADPH oxidase (Nox/Duox) family of enzymes. *BMC Evol. Biol.* **7,** 109 CrossRef Medline
31. Beaumel, S., Grunwald, D., Fieschi, F., and Stasia, M. J. (2014) Identification of NOX2 regions for normal biosynthesis of cytochrome b_{558} in phagocytes highlighting essential residues for p22phox binding. *Biochem. J.* **464,** 425–437 CrossRef Medline
32. Taylor, R. M., Burritt, J. B., Baniulis, D., Foubert, T. R., Lord, C. I., Dinauer, M. C., Parkos, C. A., and Jesaitis, A. J. (2004) Site-specific inhibitors of NADPH oxidase activity and structural probes of flavocytochrome *b*:

characterization of six monoclonal antibodies to the p22phox subunit. *J. Immunol.* **173,** 7349–7357 CrossRef Medline
33. Vlachantoni, D., Bramall, A. N., Murphy, M. P., Taylor, R. W., Shu, X., Tulloch, B., Van Veen, T., Turnbull, D. M., McInnes, R. R., and Wright, A. F. (2011) Evidence of severe mitochondrial oxidative stress and a protective effect of low oxygen in mouse models of inherited photoreceptor degeneration. *Hum. Mol. Genet.* **20,** 322–335 CrossRef Medline
34. Taylor, W. R., Jones, D. T., and Segal, A. W. (1993) A structural model for the nucleotide binding domains of the flavocytochrome b-245 β-chain. *Protein Sci.* **2,** 1675–1685 CrossRef Medline
35. Fiser, A., Do, R. K., and Sali, A. (2000) Modeling of loops in protein structures. *Protein Sci.* **9,** 1753–1773 CrossRef Medline
36. Zhu, Y., Marchal, C. C., Casbon, A. J., Stull, N., von Löhneysen, K., Knaus, U. G., Jesaitis, A. J., McCormick, S., Nauseef, W. M., and Dinauer, M. C. (2006) Deletion mutagenesis of p22^{phox} subunit of flavocytochrome b_{558}: identification of regions critical for gp91^{phox} maturation and NADPH oxidase activity. *J. Biol. Chem.* **281,** 30336–30346 CrossRef Medline
37. Meijles, D. N., Howlin, B. J., and Li, J. M. (2012) Consensus *in silico* computational modelling of the p22phox subunit of the NADPH oxidase. *Comput. Biol. Chem.* **39,** 6–13 CrossRef Medline
38. Hayes, P., Dhillon, S., O'Neill, K., Thoeni, C., Hui, K. Y., Elkadri, A., Guo, C. H., Kovacic, L., Aviello, G., Alvarez, L. A., Griffiths, A. M., Snapper, S. B., Brant, S. R., Doroshow, J. H., Silverberg, M. S., *et al.* (2015) Defects in NADPH oxidase genes NOX1 and DUOX2 in very early onset inflammatory bowel disease. *Cell Mol. Gastroenterol. Hepatol.* **1,** 489–502 CrossRef Medline
39. de Vries, S. J., van Dijk, M., and Bonvin, A. M. (2010) The HADDOCK web server for data-driven biomolecular docking. *Nat. Protoc.* **5,** 883–897 CrossRef Medline
40. van Dijk, A. D., and Bonvin, A. M. (2006) Solvated docking: introducing water into the modelling of biomolecular complexes. *Bioinformatics* **22,** 2340–2347 CrossRef Medline
41. Aoyama, T., Paik, Y. H., Watanabe, S., Laleu, B., Gaggini, F., Fioraso-Cartier, L., Molango, S., Heitz, F., Merlot, C., Szyndralewiez, C., Page, P., and Brenner, D. A. (2012) Nicotinamide adenine dinucleotide phosphate oxidase in experimental liver fibrosis: GKT137831 as a novel potential therapeutic agent. *Hepatology* **56,** 2316–2327 CrossRef Medline
42. Laleu, B., Gaggini, F., Orchard, M., Fioraso-Cartier, L., Cagnon, L., Houngninou-Molango, S., Gradia, A., Duboux, G., Merlot, C., Heitz, F., Szyndralewiez, C., and Page, P. (2010) First in class, potent, and orally bioavailable NADPH oxidase isoform 4 (Nox4) inhibitors for the treatment of idiopathic pulmonary fibrosis. *J. Med. Chem.* **53,** 7715–7730 CrossRef Medline
43. Heumüller, S., Wind, S., Barbosa-Sicard, E., Schmidt, H. H., Busse, R., Schröder, K., and Brandes, R. P. (2008) Apocynin is not an inhibitor of vascular NADPH oxidases but an antioxidant. *Hypertension* **51,** 211–217 CrossRef Medline
44. Petrônio, M. S., Zeraik, M. L., Fonseca, L. M., and Ximenes, V. F. (2013) Apocynin: chemical and biophysical properties of a NADPH oxidase inhibitor. *Molecules* **18,** 2821–2839 CrossRef Medline
45. Gianni, D., Taulet, N., Zhang, H., DerMardirossian, C., Kister, J., Martinez, L., Roush, W. R., Brown, S. J., Bokoch, G. M., and Rosen, H. (2010) A novel and specific NADPH oxidase-1 (Nox1) small-molecule inhibitor blocks the formation of functional invadopodia in human colon cancer cells. *ACS Chem. Biol.* **5,** 981–993 CrossRef Medline
46. Borbély, G., Szabadkai, I., Horváth, Z., Markó, P., Varga, Z., Breza, N., Baska, F., Vántus, T., Huszár, M., Geiszt, M., Hunyady, L., Buday, L., Orfi, L., and Kéri, G. (2010) Small-molecule inhibitors of NADPH oxidase 4. *J. Med. Chem.* **53,** 6758–6762 CrossRef Medline
47. Jaquet, V., Marcoux, J., Forest, E., Leidal, K. G., McCormick, S., Westermaier, Y., Perozzo, R., Plastre, O., Fioraso-Cartier, L., Diebold, B., Scapozza, L., Nauseef, W. M., Fieschi, F., Krause, K. H., and Bedard, K. (2011) NADPH oxidase (NOX) isoforms are inhibited by celastrol with a dual mode of action. *Br. J. Pharmacol.* **164,** 507–520 CrossRef Medline
48. Piirilä H., Väliaho J., and Vihinen M. (2006) Immunodeficiency mutation databases (IDbases). *Hum. Mutat.* **27,** 1200–1208 CrossRef Medline
49. Li, W., Cowley, A., Uludag, M., Gur, T., McWilliam, H., Squizzato, S., Park, Y. M., Buso, N., and Lopez, R. (2015) The EMBL-EBI bioinformatics web and programmatic tools framework. *Nucleic Acids Res.* **43,** W580–W584 CrossRef Medline
50. Phillips, J. C., Braun, R., Wang, W., Gumbart, J., Tajkhorshid, E., Villa, E., Chipot, C., Skeel, R. D., Kalé, L., and Schulten, K. (2005) Scalable molecular dynamics with NAMD. *J. Comput. Chem.* **26,** 1781–1802 CrossRef Medline
51. Humphrey, W., Dalke, A., and Schulten, K. (1996) VMD: visual molecular dynamics. *J. Mol. Graph.* **14,** 33–38, 27–28 CrossRef Medline